Pressure Profiles Along an Abrupt 4:1 Planar Contraction

Phillip J. Doerpinghaus and Donald G. Baird
Dept. of Chemical Engineering, Virginia Polytechnic Institute and State University, Blacksburg, VA 24061

The ability to accurately predict the pressure profile along an abrupt 4:1 planar contraction is investigated. Predicted pressure profiles obtained using the Phan Thien and Tanner (PTT) and generalized Newtonian fluid (GNF) models are compared to experimental measurements for low-density polyethylene (LDPE) and linear low-density polyethylene (LLDPE) polymer melts. The results obtained for the extensional strain hardening, LDPE resin show that numerical predictions are consistently less than the experimental values by 10–15%. Furthermore, no significant difference between the PTT and GNF predictions were observed over the range of convergent solutions. On the other hand, the numerical predictions for the LLDPE melt were within 1.5–7% of the experimental values over the entire range of stable flow rates investigated. Again, the differences in accuracy of the PTT and GNF models were small. In fact, the GNF model was generally more accurate than the PTT model for the case of LLDPE. Closer investigation of the predicted streamlines patterns near the contraction clearly shows larger, more intense vortices for the extensional strain hardening LDPE than for the LLDPE melt, which is in agreement with experimental observations. However, analysis of the plane of symmetry shows that the magnitude of the planar extensional stress is mitigated by the fluid relaxation behavior as the melt briefly passes through the contraction region. Although it appears that a viscoelastic constitutive equation is not necessary for predicting the pressure profile along an abrupt 4:1 planar contraction, this is a fortuitous result of the small extensional deformations observed in the contraction region over the limited range of convergent solutions.

Introduction

The presence of an abrupt contraction during pressure-driven flow of molten polymers gives rise to an additional pressure drop associated with the stretching of fluid elements in the vicinity of the contraction. This additional pressure drop is manifested under creeping flow conditions ($Re \sim 0$) and is often referred to as the *entrance pressure drop* (ΔP_{ent}). Figure 1 presents the pressure profile along a contraction. The magnitude of ΔP_{ent}, and the resulting increase in the driving pressure, is expected to depend upon the contraction geometry (that is, contraction ratio, contraction angle, and so on), but also appears to be sensitive to the extensional rheological properties of the material investigated (Laun and Schuch, 1989).

Surprisingly, most experimental and numerical investigations of contraction flow behavior have focused on the subtleties of the flow kinematics in the contraction region (Boger, 1987; White et al., 1987). Much of the interest in contraction flows has centered on the velocity fields, streamline patterns, and principal stress fields in relation to numerical predictions (see, for example, Luo and Mitsoulis, 1990; Park et al., 1992; and Martyn et al., 2000). Unfortunately, these past studies did not investigate measurements of the hydrodynamic pressure, which may be the most significant factor in the design of extrusion dies. Although detailed studies of the flow kinematics are important in assessing the accuracy of a numerical technique, the question of whether the pressure profile can be accurately predicted has been largely ignored.

Historically, the abrupt 4:1 contraction has been the contraction geometry of choice for analyzing the influence of viscoelastic properties on polymeric flow phenomena [see, for example, Tanner and Walters (1998)]. This flow geometry is quite simple, yet manifests mixed flow kinematics. In particu-

Correspondence concerning this article should be addressed to D. S. Baird.

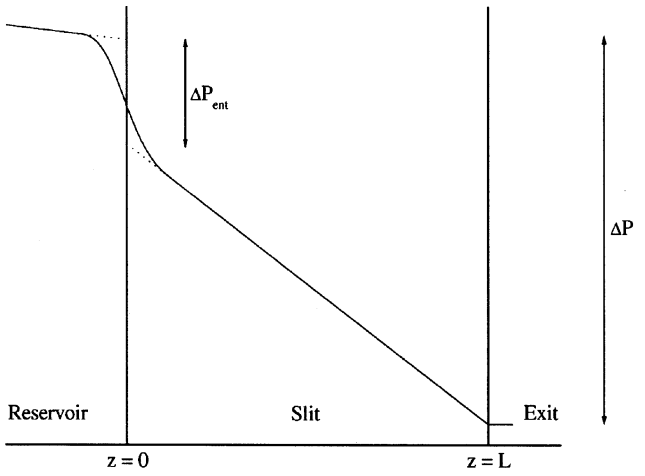

Figure 1. Hydrodynamic pressure profile along an abrupt planar contraction; the magnitude of ΔP_{ent} has been exaggerated for effect.

lar, simple shear flow dominates the regions well upstream and downstream of the contraction, while the contraction region is greatly influenced by extensional deformations. One of the most unique flow characteristics arising from contraction flow is the presence of recirculating vortices in the reentrant corner regions. During stable flow conditions, natural tapering of the bulk flow into the contraction leads to "dead" regions where vortices are manifested. This natural tapering effectively reduces the cross-sectional area of flow upstream of the contraction and contributes to the observed entrance pressure drop. Studies by Ballenger and White (1970), den Otter (1970), and White and Baird (1986), to name a few, have found that not all polymer melts exhibit vortex formation. Specifically, Ballenger and White found that highly long-chain branched low-density polyethylene (LDPE) exhibited substantial vortex growth, while linear high-density polyethylene (HDPE) did not. Similar results were observed by den Otter for branched and linear polydimethylsiloxane (PDMS) resins. White and Baird (1986) investigated the streamlines of LDPE and polystyrene (PS) and found that flow tapering was related to the degree of extensional strain hardening and the intensity of the vortices was determined by the shear thinning behavior. Highly branched LDPE, exhibiting considerable extensional strain hardening and shear thinning behavior, showed significant tapering and intense vortices. These observations indicate that flow tapering, recirculating vortices, and possibly the magnitude of ΔP_{ent}, are strongly influenced by the melt rheological properties.

The extensional flow characteristics of long-chain branched polymers, such as LDPE, are substantially different from linear polymers (Laun and Schuch, 1989). Highly branched polymers exhibit extensional strain-hardening behavior, which contrasts to the strain-softening behavior often observed in linear polymers. Strain hardening refers to the rise in extensional viscosity above the linear viscoelastic limit of $3\eta^+(t)$. Previous studies have shown that the magnitude of strain hardening in randomly branched LDPE resins is influenced by the degree of branching (White, 1978; Münstedt and Laun, 1981; Minoshima and White, 1986). Interestingly, linear resins having broad molecular-weight distributions, or the presence of very high molecular-weight species can also exhibit some degree of extensional strain hardening (Münstedt, 1980; Frank and Meissner, 1984). Therefore, accurate modeling of the extensional behavior of the polymer melt would seem important when trying to predict the presence of tapered flow and its effect on the pressure profile.

The question, however, is whether one needs to use a viscoelastic constitutive equation to model the pressure drop across a 4:1 contraction or whether a purely viscous constitutive equation is accurate enough. The simplest rheological constitutive equation used to describe polymer melts is the inelastic generalized Newtonian fluid (GNF) model. Although capable of describing the shear-thinning nature of polymer melts, the GNF model does not capture viscoelastic phenomena such as fluid memory, normal stress differences, and extensional strain-hardening behavior. On the other hand, viscoelastic constitutive equations such as the Phan Thien/Tanner (PTT) and factorized K-BKZ models are known to accurately describe nonlinear rheological phenomena (Phan Thien and Tanner, 1977; Kaye, 1962; Bernstein et al., 1963). Both the PTT and K-BKZ models can accurately describe shear thinning, normal stress differences, and extensional strain-hardening behavior in uniaxial extension. This is especially important when predicting free surface flows, such as extrudate swell. The major weakness of using the K-BKZ model is that it cannot accurately predict simultaneously both shear thinning and planar extensional strain hardening using traditional damping functions (Samurkas et al., 1989; Ahmed and Mackley, 1995). As a result, its use in planar contraction geometries is limited. More recently, McLeish and Larson (1998) have developed the pom-pom constitutive model that specifically addresses the effects of long-chain branching on extensional viscosity. The pom-pom model is capable of predicting extensional strain hardening in both uniaxial and planar extension. Unfortunately, the large number of model parameters and the arbitrary nature by which they are chosen can limit its implementation in numerical simulations at present.

Recently, numerical simulations using a variety of constitutive equations concerned with the prediction of the entrance pressure drop across axisymmetric contraction geometries have been reported. Hatzikiriakos and Mitsoulis (1996) studied the Bagley end correction of linear low-density polyethylene (LLDPE) both experimentally and numerically using the K-BKZ/PSM (Papanastasio et al., 1983) constitutive equation. They found that the numerical simulations significantly underestimated the experimental observations. Similar results were reported by Mitsoulis and coworkers (1998) and by Barakos and Mitsoulis (1995) for LLDPE and LDPE resins, respectively. Beraudo et al. (1996) investigated the Bagley end correction for LLPDE using the multimode PTT constitutive model and found that numerical simulations underpredicted the experimentally measured ΔP_{ent} by a factor of 2 at low rates and by a factor of 4 at high rates. Interestingly, Mitsoulis et al. (1998) found that the entrance pressure-drop loss predicted by the K-BKZ model was insensitive to the extensional characteristics over the range of rates and model parameters used in their study. In fact, an inelastic GNF constitutive model was found to provide similar results for ΔP_{ent} to the more complex viscoelastic constitutive equation. This ob-

servation indicates that the use of a viscoelastic constitutive equation may not be required under certain flow conditions.

Although measurements of ΔP_{ent} are useful and are believed to provide an indication of the extensional character of the fluid (Cogswell, 1972; Binding, 1988), the method used to calculate these quantities often leads to a significant uncertainty. The most common method for determining ΔP_{ent} is by applying the Bagley end correction (Bagley, 1957). This method involves extrapolating the measured pressure drop across multiple capillaries of the same diameter and differing length to a L/D of zero. This extrapolated quantity then represents ΔP_{ent} for the given contraction ratio. The effects of pressure, viscous heating, and wall slip can also contribute to substantial error in the value of ΔP_{ent}. Although the use of a very short die ($L/D \sim 0$) mitigates these effects, the relatively small measurable pressure drop can also lead to significant uncertainty. In order to avoid uncertainties associated with explicitly calculating ΔP_{ent}, measurement of the hydrodynamic pressure along the contraction geometry should provide more accurate results. This approach addresses the effects of ΔP_{ent} on the upstream pressure measurements while reducing the uncertainty associated with extrapolating experimental measurements. This technique also simplifies the application of numerical predictions by eliminating the need to extrapolate predicted pressure profiles to the contraction entrance.

The objective of the current study is to determine the role that viscoelasticity, and more importantly extensional strain hardening, has on the flow behavior of polymer melts through an abrupt planar contraction. This is accomplished by comparing experimentally measured pressure profiles along a 4:1 planar contraction die to predictions obtained from the finite-element method (FEM) numerical simulations. Two well-characterized polyethylene resins having different shear and extensional flow characteristics will be investigated in this study. A multimode PTT model and an inelastic GNF model will be used to model the rheological characteristics of each polyethylene and predict the pressure profiles along the chosen 4:1 planar contraction geometry. Comparing the PTT and GNF predictions will isolate the specific role of fluid memory and extensional strain hardening on the pressure-profile predictions. Predicted streamline patterns and the planar extensional strain rates and stresses along the plane of symmetry will be used to further compare the influence of viscoelasticity and extensional strain hardening.

Constitutive Equations

The viscoelastic and inelastic constitutive equations used in this study are briefly outlined in this section. The reader should note that the following equations have been formulated using the convention described by Bird et al. (1987), in which a tensile stress is taken to be negative.

Phan Thien and Tanner model

The (PTT) model was chosen to describe the viscoelastic properties of the polyethylene resins utilized in this study. The PTT model is a differential constitutive model based on network theory of concentrated polymer solutions and melts (Phan Thien and Tanner, 1977; Phan Thien, 1978). A multimode formulation using the exponential coefficient appears as

$$\boldsymbol{\tau} = \sum_i \tau_i \tag{1}$$

$$\exp\left(-\frac{\epsilon\lambda_i}{\eta_i} tr\boldsymbol{\tau}_i\right)\tau_i + \lambda_i \boldsymbol{\tau}_{i(1)} + \xi\lambda_i\left(\dot{\boldsymbol{\gamma}}\cdot\boldsymbol{\tau}_i + \boldsymbol{\tau}_i\cdot\dot{\boldsymbol{\gamma}}\right) = -\eta_i\dot{\boldsymbol{\gamma}} \tag{2}$$

where $\dot{\boldsymbol{\gamma}}$ is the rate of deformation tensor and $\boldsymbol{\tau}_{i(1)}$ is the upper-convected derivative of stress for the ith mode and are defined by

$$\dot{\boldsymbol{\gamma}} = \nabla\boldsymbol{\nu} + (\nabla\boldsymbol{\nu})^{\dagger} \tag{3}$$

$$\boldsymbol{\tau}_{i(1)} = \frac{\partial\boldsymbol{\tau}}{\partial t} + \boldsymbol{\nu}\cdot\nabla\boldsymbol{\tau}_i - \left(\dot{\boldsymbol{\gamma}}\cdot\boldsymbol{\tau}_i + \boldsymbol{\tau}_i\cdot\dot{\boldsymbol{\gamma}}\right) \tag{4}$$

The extra stress $\boldsymbol{\tau}$ is calculated from the sum of the individual extra stresses for each mode, $\boldsymbol{\tau}_i$; and λ_i and η_i correspond to the relaxation time and viscosity for the ith mode, respectively. In addition to the usual linear viscoelastic constants, two nonlinear parameters are also used: ϵ characterizes the rate of destruction of entanglement "cross-links" in the network model, and ξ denotes the rate of nonaffine deformation. In this study, single values of ϵ and ξ common to all modes have been used.

Generalized Newtonian fluid (GNF) model

In addition to a viscoelastic constitutive model, a generalized Newtonian fluid (GNF) model was also used. The GNF model predicts the shear viscosity according to a specified viscosity model, and predicts a uniaxial extensional viscosity that is three times greater than the shear viscosity and a planar extensional viscosity that is four times greater. An inelastic, purely viscous constitutive model was chosen to contrast the effects of memory and nonlinear extensional properties. The viscosity model chosen to best describe the shear-thinning nature of both polymer fluids was the Carreau-Yasuda (C-Y) model (Carreau, 1968; Yasuda et al., 1981). The GNF constitutive equation and the Carreau-Yasuda viscosity model can be expressed as

$$\boldsymbol{\tau} = -\eta(\dot{\gamma})\dot{\boldsymbol{\gamma}} \tag{5}$$

$$\eta(\gamma) = (\eta_0 - \eta_\infty)\left[1 + (\lambda\gamma)^a\right]^{(n-1)/a} + \eta_\infty \tag{6}$$

where η_0 and η_∞ are the zero-shear and infinite-shear viscosities, respectively, λ is a time constant, n is the power-law index, and a is a dimensionless parameter that describes the transition region between the zero-shear and power-law regions. The scalar quantity $\dot{\gamma}$ represents the magnitude of the rate of strain tensor $\dot{\boldsymbol{\gamma}}$ and is defined by

$$= \sqrt{1/2\,\dot{\boldsymbol{\gamma}}:\dot{\boldsymbol{\gamma}}} \tag{7}$$

Table 1. Molecular Weight, MFI, and LCB Content of the Materials Studied

Resin	ρ (g/cm^3)	MFI (dg/min)	M_w	M_w/M_n	M_z	LCB /10^4C
NA952	0.918	2.0	235,500	17.1	2,619,300	39*
NTX101	0.917	0.9	122,700	3.44	319,700	—

*C^{13} NMR measurement.

Experimental Methods

Materials

Two commercial-grade polyethylenes were investigated in this study: a LDPE produced by Equistar Chemical under the product name NA952 and a LLDPE produced by Exxon-Mobil under the product name NTX101. The LDPE is a tubular reactor polymerized polyethylene having a high degree of short- and long-chain branches. The LLDPE is an ethylene–hexene copolymer produced using conventional Ziegler-Natta catalysts. Neither of the resins investigated contain slip or antiblock agents that might obscure their flow properties.

The relevant physical and molecular properties are tabulated in Table 1. The LDPE resin has a very large weight-average molecular weight of 235,500 g/mol and a broad molecular-weight distribution of 17.1. These values are characteristic of highly branched polyethylenes. The degree of long-chain branching obtained from C^{13} NMR analysis was estimated to be 3.9 long-chain branches per 1,000 carbons. The LLDPE has a more modest M_w of 112,800 g/mol and a relatively narrow molecular weight distribution of 3.41. No long-chain branches are present in the structure of the NTX101 resin.

Rheological testing

The shear rheological measurements for each resin were determined using a Rheometrics Mechanical Spectrometer Model 800 (RMS-800). The shear viscosity curves for each PE resin are presented in Figure 2. The dynamic oscillatory data were collected over the frequency range of 0.1–100 rad s^{-1} using 25-mm parallel plate fixtures. The steady shear rheological measurements were collected over the shear rate range of 0.001–1.0 s^{-1} using a 25-mm cone-and-plate fixture. The cone angle used for all steady shear measurements was 0.1 rad. All testing was preformed within an inert nitrogen atmosphere to prevent thermooxidative degradation. In most cases, the test samples were prepared by compression molding preformed at 170°C under nominal pressure and allowing them to cool slowly. All steady shear and dynamic oscillatory measurements were acquired at a test temperature of 150°C. The results presented represent an average of at least three runs using different samples each time. The calculated error for the dynamic oscillatory and steady shear measurements was found to be no greater than ± 5 and $\pm 10\%$, respectively.

High shear-rate viscosity data were collected using a Goettfert Rheograph 2001 (RG2001) capillary rheometer. The high shear-rate rheological measurements were collected over the range of 10–100 s^{-1}. Three capillaries with a diameter of 1.0 mm and L/D ratios of 10, 20, and 30 were used for measurements performed at temperatures of 150°C. Using the Rabinowitsch correction to calculate the true wall shear rate and the Bagley end correction to calculate the true wall shear stress, the shear viscosity as a function of shear rate was calculated from the imposed volumetric flow rate and the resulting pressure drop. These data were used exclusively to determine the PTT constitutive model parameter ξ and can be found presented elsewhere (Doerpinghaus, 2002).

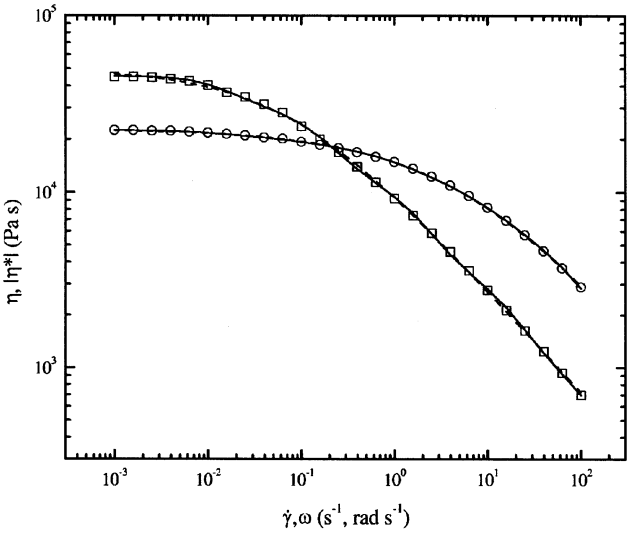

Figure 2. Steady and dynamic oscillatory viscosity measurements obtained at $T = 150$°C.

Experimental measurements: (□) LDPE, (○) LLDPE; Numerical Predictions: (——) PTT, (— — —) GNF.

Uniaxial extensional stress growth measurements were obtained using a Rheometrics Extensional Rheometer Model 9000 (RER-9000). This particular extensional rheometer is based upon the design of Münstedt (1979). The transient extensional data were collected over the extension-rate range of 0.01–1.00 s^{-1}. Extensional viscosity measurements obtained at $\dot{\epsilon} = 1.0$ s^{-1} are presented in Figure 3. The maximum Hencky (true) strain achievable with this device is approximately 3.0 using test specimens with initial nominal lengths of 22 mm. The cylindrical test specimens are compression molded from polymer pellets at 170°C under nominal pressure and allowed to cool slowly. They were then bonded to test clips using high-temperature UHU epoxy, mounted to the rheometer, and immersed in a neutrally buoyant silicone oil bath at 150°C. Once thermal equilibrium was achieved, an applied extension rate deformed the sample, and the resulting force was monitored using a leaf spring–LVDT assembly. The results presented for each extension rate represent an average of at least three runs using different samples. The calculated error for the extensional viscosity data was found to be less than $\pm 10\%$.

Flow system

The abrupt planar contraction die utilized in this study consists of two halves machined from 440C stainless steel. When bolted together, the desired flow channel is formed. Figure 4 shows the contraction die. The flow channel is 12.7

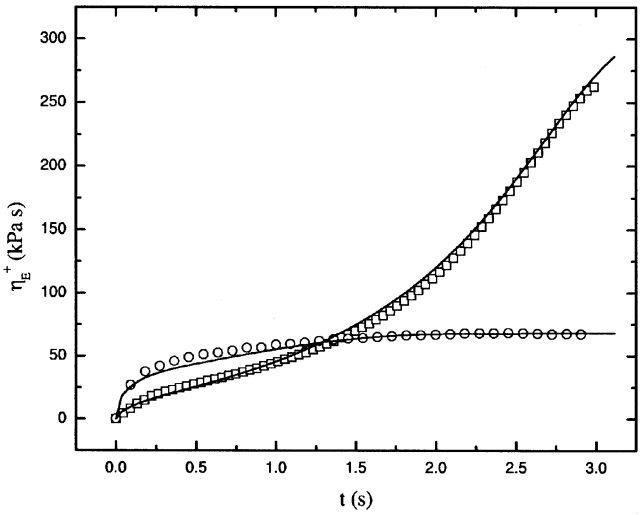

Figure 3. Transient, uniaxial extensional viscosity measurements for $\dot{\epsilon} = 1.0\ s^{-1}$ at $T = 150°C$.

Experimental measurements: (□) LDPE, (○) LLDPE; Numerical predictions: (——) PTT model.

mm wide and is divided into two regions. The upstream region is 108 mm long and 5.08 mm high. The downstream region is 25.4 mm long and 1.27 mm high. This results in a 4:1 contraction ratio, $L_{res}/H_{res} = 21.2$ and $L/H = 20$. While the downstream region has an aspect ratio (W/H) of 10, the upstream aspect ratio is 2.5 and represents a departure from true planar flow conditions.

Six pressure transducer ports were machined along the flow channel of the die (Figure 4). The four upstream transducer ports were machined flush with the channel wall, while the two downstream transducer ports were machined at the bottom of deep pressure holes. Although the use of pressure holes can lead to error in the measurement of the hydrodynamic pressure, a previous study using similar polymer melts showed that the magnitude of the error does not exceed $\pm 5\%$ of the absolute pressure (Chang, 1986). During operation, Dynisco melt pressure transducers ranging from 3.45 MPa to 10.3 MPa (500–1,500 psig) were used to monitor the hydrodynamic pressure. The calculated error for the experimental pressure measurements was found to be $\pm 2\%$ at the nominal apparent shear rate cited.

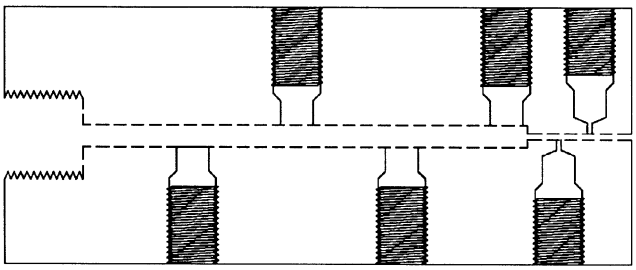

Figure 4. Abrupt 4:1 planar contraction profiling die used in this study.

Pressure tap centers are located at $z = -81, -56, -30, -5$, 8, and 15 mm from the planar contraction ($z = 0$).

Table 2. PTT Model Parameters

λ_i	η_i (LDPE)	η_i (LLDPE)
10^{-2}	8.50×10^2	3.83×10^3
10^{-1}	2.38×10^3	6.36×10^3
10^{0}	7.78×10^3	7.37×10^3
10^{1}	1.78×10^4	2.89×10^3
10^{2}	1.67×10^4	2.09×10^3
ξ	0.191	0.179
ϵ	0.034	0.239

The polymer melt was supplied to the planar contraction die using an extruder–gear pump assembly. The polymer was first plasticated using a 25.4-mm Killion laboratory extruder and then fed to a Zenith (HPB-5556) gear pump operating at 150°C. A 1/4 hp U.S. Motors Varidrive ac motor coupled to a Reynold Ltd. 21.4:1 gear-reduction unit was used to drive the gear pump. This arrangement provides precise, pulseless flow of polymer over the volumetric flow-rate range of 15.0–150 mm^3/s.

Numerical Methods

Model parameter fitting

The Phan Thien and Tanner (PTT) model parameters were determined from shear and extensional viscosity data. Table 2 summarizes the PTT model parameters obtained for the LDPE and LLDPE resins. The discrete relaxation spectra (λ_i, η_i) were obtained from nonlinear regression of the homogeneous, steady shear, and dynamic oscillatory measurements. Arbitrary values of λ_i were chosen over the range of data available. The nonlinear parameter ξ was determined from shifting the dynamic viscosity (η') to overlay the steady shear viscosity (η) in the non-Newtonian flow regime. Finally, the ϵ parameter was determined from transient extensional data at the highest extension rate of 1.0 s^{-1} using a least-square optimization technique (Doerpinghaus, 2002). The corresponding fits to rheological data are found in Figures 2 and 3.

The C-Y viscosity model parameters were determined from shear viscosity data alone. The C-Y parameters for each resin are tabulated in Table 3. The value of η_0 was empirically determined from available rheological data, and η_∞ was assumed to be approximately zero. The choice of η_∞ had little influence on the other parameters. The remaining parameters were determined from nonlinear regression of available data. The corresponding fit to the shear viscosity data is found in Figure 2.

Finite-element method

The FEM was employed to solve simultaneously the governing equations for isothermal, inertialess flow of incom-

Table 3. GNF Model Parameters

	LDPE	LLDPE
η_0	49,430	22,740
λ_∞	0	0
λ	12.5	0.130
n	0.409	0.336
a	0.625	0.487

pressible viscoelastic fluids. The equations of continuity and motion for incompressible, creeping flow can be written in the following forms, respectively

$$\nabla \cdot \boldsymbol{\nu} = 0 \tag{8}$$

$$\nabla \cdot \boldsymbol{\tau} + \nabla P = 0 \tag{9}$$

where ∇ is the gradient operator, $\boldsymbol{\nu}$ is the velocity field, $\boldsymbol{\tau}$ is the extra stress tensor, and P is the modified pressure. In order to close the equation set, one of the two rheological constitutive equations described earlier must also be used.

The commercial FEM package Polyflow (Fluent/Polyflow s.a., version 3.8) was used to perform all numerical simulations on a dedicated SGI Origin 200 server. The viscoelastic predictions were determined using the elastic viscous split stress (EVSS) technique (Rajagopalan et al., 1990) coupled with inconsistent streamline upwinding (SU) (Marchal and Crochet, 1987). This particular approach reduces the computational expense and enhances the range of convergence for multimode viscoelastic simulations. On the other hand, the GNF predictions were determined using Newton iterations upon the locally calculated viscosities. For both fluid descriptions, quadratic, continuous (P^2-C^0) interpolation of the velocity field and linear, continuous (P^1-C^0) interpolation of the pressure field are utilized. Here, the superscripts refer to the order the polynomial P used to interpolate the solution and the piecewise continuity C between elements. Linear, continuous (P^1-C^0) interpolation of the stress field was also used in the viscoelastic predictions.

Because the governing equations for viscoelastic fluid result in a set of highly nonlinear equations, a convergent solution cannot be obtained in a single step. The parameters leading to nonlinearity must be incremented gradually, or evolved. For this study, the volumetric flow rate (Q_{2D}) has been chosen as the evolution parameter. The initial flow rate is chosen such that the fluid is Newtonian in nature. Once a solution is obtained, the flow rate is gradually increased using the previous solution as an initial guess for the next evolutive step. This process gradually builds the elastic contribution into the predictions. Furthermore, each intermediate solution has physical significance because the fluid properties have not been changed, merely the volumetric flow rate. Once a convergent solution is obtained for the flow rate of interest, the simulation is concluded.

Computational mesh

The finite-element mesh used to describe the abrupt contraction geometry is found in Figure 5. This mesh contains 992 elements and 1113 nodes. The influence of mesh refinement on the convergence of the solution has been investigated (Doerpinghaus, 2002) but is not shown here for clarity. The finite-element mesh used in this study was found to be essentially independent of element size, and provided convergent solutions with the least computational expense.

The boundary conditions applied to the finite-element mesh were as follows: fully developed flow ($v_2 = 0$, flow rate Q) at inflow, no slip ($v_1 = v_2 = 0$) along the wall, fully developed flow ($v_2 = 0$, flow rate Q) at outflow, and planar symmetry ($f_1 = 0$, $v_2 = 0$) along the center line. Here, v is defined as the velocity and f as the force. The subscripts 1 and 2 refer to the flow direction and normal direction, respectively. Additionally, a value of zero was assigned to the pressure field at the die exit, adjacent to the wall. Although there exists some uncertainty in the exit pressure due to exit flow phenomena, pressure measurements at the die exit are impractical, extrapolation of the measured pressure field proves to be subjective (Tuna and Finlayson, 1988), and the lack of die swell measurements precludes free-surface profile matching.

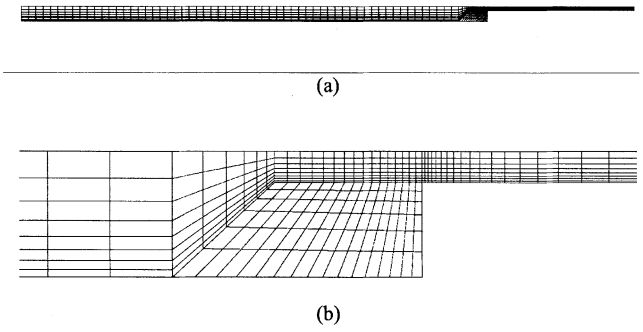

Figure 5. Computational finite-element mesh: (a) full mesh domain; (b) expanded view of the entry region.

Results and Discussion

In this section, the pressure profiles, streamline patterns, and center-line predictions obtained from numerical simulations will be presented and discussed. The imposed volumetric flow rate will be identified by the apparent wall shear rate defined as

$$\dot{\gamma}_a = \frac{6Q}{WH^2} \tag{10}$$

where Q is the imposed volumetric flow rate, W is the channel width, and H is the downstream full channel height. Furthermore, at each simulated flow rate the relative elastic contribution will be determined from the dimensionless Weissenberg number, *We*. Because multimode constitutive model formulations complicate the determination of the fluid characteristic relaxation time, the following definition has been used

$$We = \frac{N_1}{2\tau_w} \tag{11}$$

where N_1 is the primary normal stress difference ($\tau_{11} - \tau_{22}$) evaluated at the wall in the downstream section and τ_w is the wall shear stress (τ_{12}) evaluated at the same location. The exact location is determined by the onset of fully developed flow. This quantity is often referred to as the stress ratio and is used as a measure for the level of numerical convergence. Alternately, many choose to define *We* as the product of the characteristic relaxation time of the fluid λ, the average fluid velocity $\langle V \rangle$, and the reciprocal of the full slit height H^{-1}. This alternate measure will also be provided (in parenthesis)

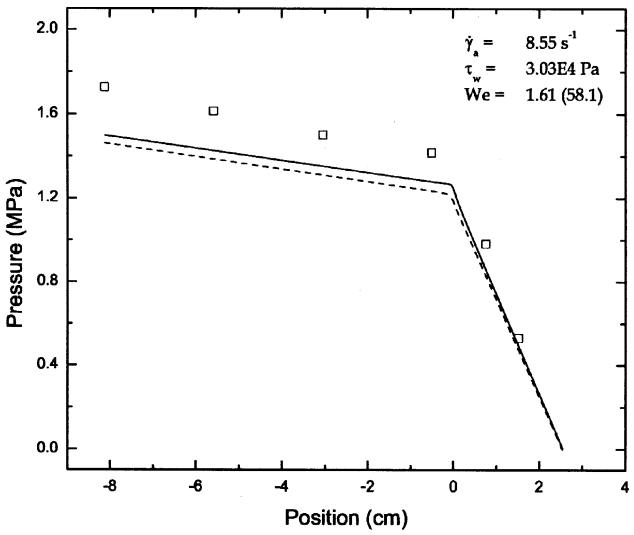

Figure 6. Pressure profile for LDPE at $\dot{\gamma}_a = 8.55\ s^{-1}$.

Experimental measurements (□), PTT predictions (——), GNF predictions (— — —).

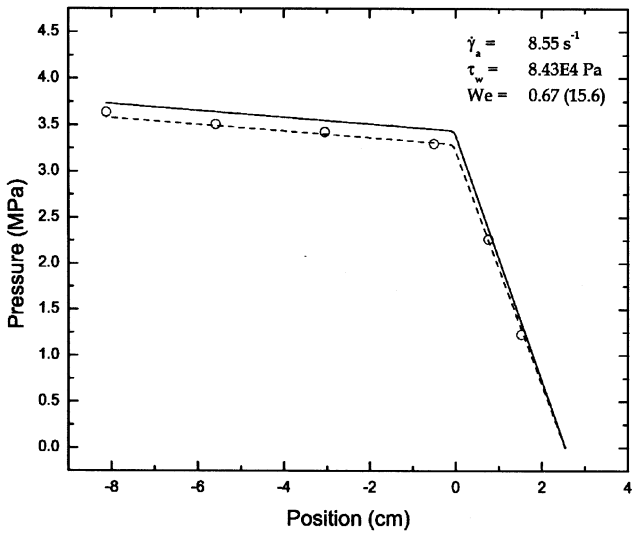

Figure 7. Pressure profile for LLDPE at $\dot{\gamma}_a = 8.55\ s^{-1}$.

Experimental measurements (○), PTT predictions (——), GNF predictions (— — —).

for reference purposes. In light of various physical flow instabilities that occur at high flow rates (that is, melt fracture), the range of convergence will be monitored against the apparent wall shear stress, τ_w.

Pressure profiles

The experimental and predicted pressure profiles for LDPE at $\dot{\gamma}_a = 8.55\ s^{-1}$ are depicted in Figure 6. The experimental pressure measurements obtained from each of the six pressure transducers mounted along the flow channel are compared to the predicted pressure profiles obtained along the plane of symmetry for both the PTT and GNF constitutive models. A number of interesting features can be addressed. First, the upstream pressure profile shows that the experimental values are generally higher than either of the predicted curves. The numerical predictions are consistently 12–14% less than the experimental values, which exceed the observed experimental error in the pressure measurements. Second, the difference between the viscoelastic and inelastic models is small at the imposed flow rate. The PTT model predicts less than a 5% increase over the GNF model predictions. This minimal increase in the observed hydrostatic pressure occurs despite $We = 1.61$ (58.1), a substantial value for *We*. In addition to the Weissenberg number, the downstream wall shear stress τ_w is also presented. With a value of only 0.03 MPa, the possible effects of the melt fracture that arise at $\tau_w > 0.1$ MPa are not a significant concern (Petrie and Denn, 1976)

Figure 7 shows the pressure profiles for LLDPE at $\dot{\gamma}_a = 8.55\ s^{-1}$. First, it can be seen that the model predictions are much more accurate for the LLDPE resin than they are for the LDPE resin. Both the PTT and GNF model predictions are within 5.0% of the experimentally measured pressures. Second, the GNF model appears to do a better job of predicting the pressure profile than the PTT model. The GNF predictions are in very good agreement with the measured profile, having an average error of only 1.4%. This overall better agreement is most likely due to the lack of significant nonlinear behavior for LLDPE. The delayed onset of shear thinning, short relaxation times, and the lack of extensional strain hardening are much more Newtonian like than the behavior exhibited by the LDPE melt. As a result, the GNF model does as good a job of describing the pressure drop through the contraction die as the PTT model. The value of *We* is also much smaller at 0.67 (15.6), but τ_w is noticeably higher at 0.08 MPa. The reduced degree of shear thinning in LLDPE contributes to this higher value of the wall shear stress.

Further increases in the imposed flow rate resulted in a loss of convergence in the numerical solutions for the PTT predictions of LDPE. Table 4 summarizes the range of flow rates investigated and the average error between experimental and numerical profiles for each fluid description. Surprisingly, the PTT predictions for LLDPE did not suffer from this limitation. PTT predictions for the LLDPE resin were obtained up to the maximum apparent shear-rate investigated of 37.0 s^{-1}. The experimental measurements of the pressure profile and the *obtainable* numerical predictions at the highest apparent shear rate are presented in Figures 8 and 9. Figure 8 compares the experimental values for LDPE at $\dot{\gamma}_a = 37.0\ s^{-1}$ to the GNF model predictions. Once again,

Table 4. Model Predictions–Average Absolute Errors

	LDPE		LLDPE	
	PTT	GNF	PTT	GNF
$\dot{\gamma}_a$	% Error	% Error	% Error	% Error
4.36	11	12	2.8	1.9
8.55	12	14	5.1	1.4
13.6	—	14	6.0	1.5
19.3	—	14	7.1	2.5
25.1	—	13	7.2	4
30.9	—	13	11	5.3
37.0	—	12	13	6.7

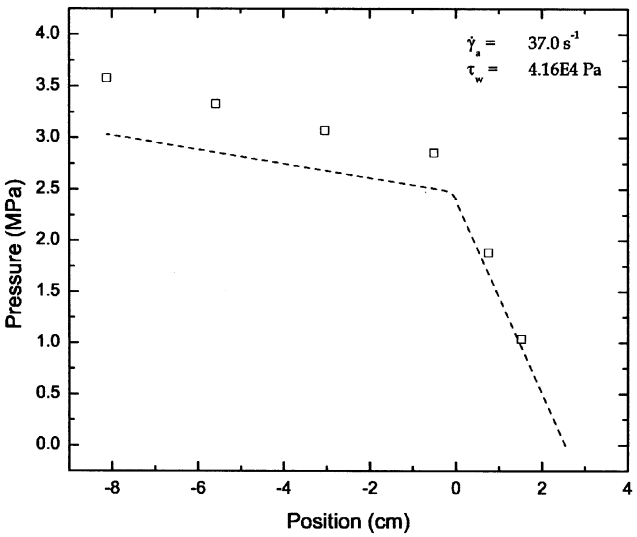

Figure 8. Pressure profile for LDPE at $\dot{\gamma}_a = 37.0\ s^{-1}$.

Experimental measurements (□), GNF predictions (— — —).

considerable underprediction is observed, with an average error of 12%. This is most likely due to poorly captured extensional characteristics that are important in the entrance region. On the other hand, Figure 9 exhibits the opposite trend for LLDPE. Now the model predictions consistently overpredict the measured pressure profiles. This reversal may at first seem inconsistent, but the calculated wall shear stress is in excess of 0.21 MPa, and surface melt fracture was observed experimentally. In this case, the presence of a finite slip velocity at the die wall associated with melt fracture may justify this decrease in the observed profile values, but experimental slip velocity measurements were not performed to confirm this.

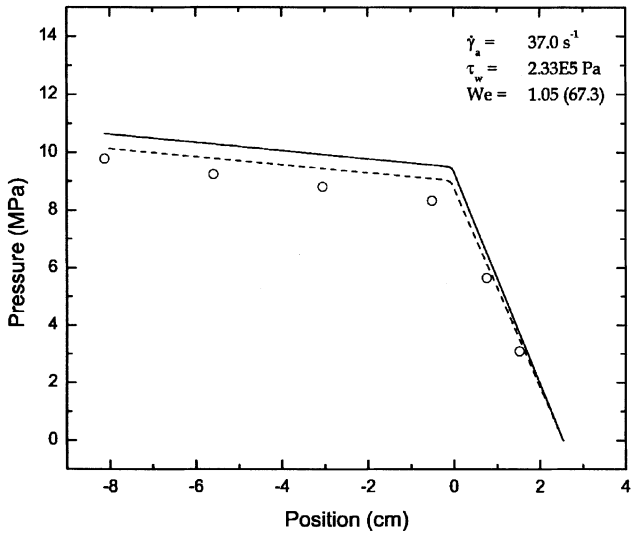

Figure 9. Pressure profile for LLDPE at $\dot{\gamma}_a = 37.0\ s^{-1}$.

Experimental measurements (○), PTT predictions (——), GNF predictions (— — —).

The results obtained from the measured and calculated pressure profiles clearly indicate that model predictions for the LLDPE resin are generally more accurate than those for the LDPE resin. The consistent underprediction of the hydrodynamic pressure along the contraction die for LDPE implies that the calculated magnitude of ΔP_{ent} is less than observed. This agrees in general with the observations of Barakos and Mitsoulis (1995) and Mitsoulis (2001). Conversely, the results obtained for LLDPE would appear to be adequate, at least to within the accuracy of the experimental pressure measurements of $\pm 2\%$. Therefore, from the standpoint of die design and processing operations, the predictions for LLDPE are adequate, while the predictions for LDPE are subject to more uncertainty.

Surprisingly, comparing the predictions obtained from the PTT and GNF models indicate that the use of a viscoelastic model may not be necessary for the 4:1 planar contraction geometry, at least with respect to pressure measurements. Within the range of convergent solutions, the differences between the predicted pressure profiles for the PTT and GNF models were found to be small in comparison to the error between predicted and experimental quantities. This trend was observed for both LDPE and LLDPE. This suggests that the shear viscosity determines the measured hydrodynamic pressure and that use of a computationally expensive, viscoelastic constitutive equation may not be necessary. Of course, this assessment only applies to the shear-rate ranges (and Weissenberg numbers) covered *numerically*.

The loss of convergence continues to be a problem for numerical simulations at high Weissenberg numbers. The highly strain-hardening LDPE was limited to a maximum apparent shear rate of 8.55 s^{-1}, corresponding to a Weissenberg number of 1.61 (58.1) and a wall shear stress of only 0.03 MPa. The exact cause for the loss of convergence is not entirely clear, but the high degree of strain hardening in the planar extension combined with the presence of a corner singularity in the flow domain may have contributed. Conversely, the convergence range for the LLDPE simulations extended over the entire range of experimental flow rates investigated. In fact, numerical predictions were obtained at flow rates and wall shear stresses beyond the observed onset of surface melt fracture.

Predicted streamline patterns

Streamline patterns were obtained in the entrance region to better understand the influence that viscoelasticity and extensional strain hardening have on the flow kinematics. Figure 10 shows the predicted streamlines obtained from PTT and GNF simulations for both LDPE and LLDPE at $\dot{\gamma}_a = 8.55\ s^{-1}$. This apparent shear rate was chosen because it represents the maximum rate for which convergent PTT predictions are available for both LDPE and LLDPE. Figure 10a presents the predictions for LDPE. Clearly, the PTT model predicts sizeable recirculating vortices in the reentrant corners and pronounced tapering of the flow into the contraction. This tapering becomes more apparent when the GNF predictions, which do not exhibit vortices, are also plotted. The streamline along the plane of symmetry as predicted by the PTT model represents $\Psi_{max} = 1.0$, and the minimum value found at the center of the vortex is $\Psi_{min} = -0.0053$. Con-

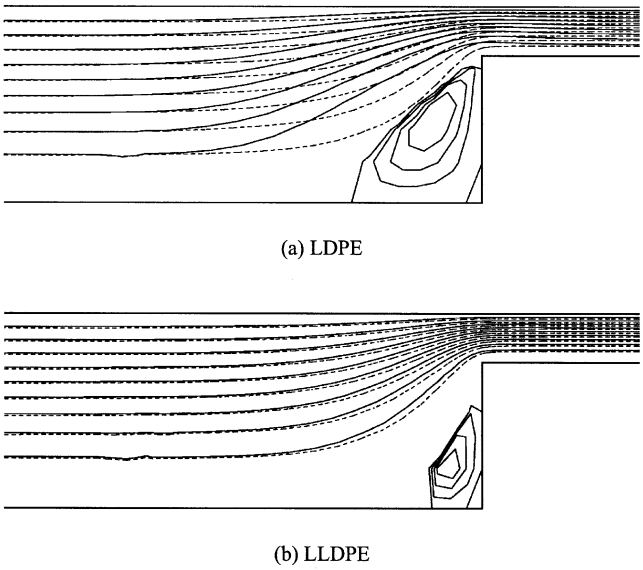

Figure 10. Streamline patterns for LDPE and LLDPE at $\dot{\gamma}_a = 8.55\ s^{-1}$.

Solid lines represent PTT predictions and dashed lines represent GNF predictions at same values of Ψ.

versely, LLDPE does not show a large degree of tapering into the contraction. Figure 10b shows that the predictions for the PTT and GNF model for LLDPE are very similar, with only slight deviations near the contraction. Although a small vortex is predicted in the PTT simulated streamlines, the minimum value of the streamline function is $\Psi_{min} = -0.0016$, which is more than three times smaller than that calculated for LDPE. This reduced intensity of the vortex has been observed for polymer melts exhibiting less shear-thinning behavior (White and Baird, 1986).

The predicted degree of flow tapering, as well as the intensity of the recirculating vortices, is dependent upon the constitutive model and the model parameters used. The streamline predictions of the PTT model for LDPE show significant vortex growth and flow tapering into the contraction. On the other hand, less tapering and diminished vortices are predicted for the LLDPE melt. Together, these results agree qualitatively with prior experimental observations and numerical simulations of linear and branched polyethylene melts (White and Kondo, 1977; Dupont and Crochet, 1988; Ahmed et al., 1995; Mitsoulis, 2001). However, one begins to realize that capturing the correct flow kinematics does not necessarily imply an accurate prediction of the hydrodynamic pressures. This observation confirms prior studies by Barakos and Mitsoulis (1995). A better assessment of the effects of viscoelasticity and extensional strain hardening may lie in the extrastress predictions.

Plane of symmetry analysis

The plane of symmetry represents the region of pure planar extensional deformation within the contraction die. Well upstream and downstream of the contraction the planar extension rate approaches zero, while the extension rate becomes significant at the contraction. In this section, the predicted extension rates and the calculated net planar stresses σ_1 $(=\tau_{11}-\tau_{22})$ will be analyzed.

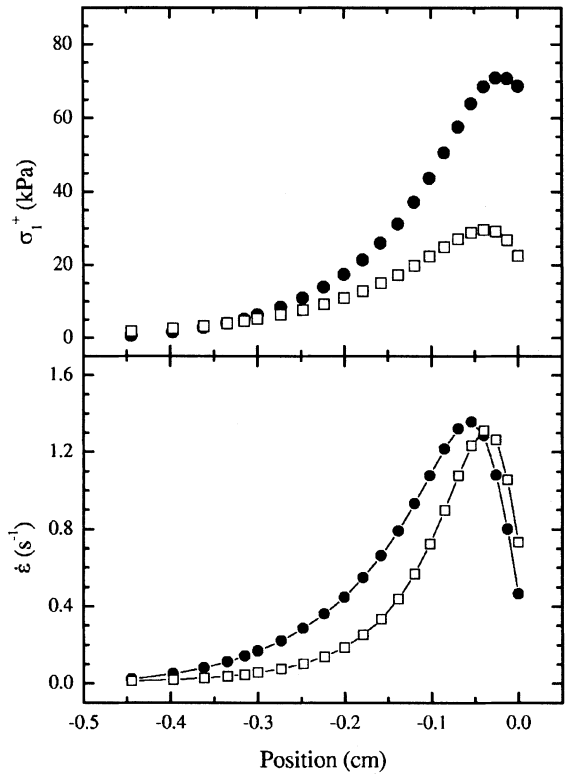

Figure 11. Predicted extension rates and extensional stresses along the plane of symmetry for LDPE at $\dot{\gamma}_a = 8.55\ s^{-1}$.

(●) PTT predictions, (□) GNF predictions. Lines have been drawn to aid the eye.

Figure 11 presents the predicted extensional characteristics of LDPE in the vicinity of the abrupt contraction. The planar extension rate and the unsteady planar stress σ_1^+ are plotted as a function of the position for both the PTT and GNF model predictions. The planar extension rates are first observed to increase at a location approximately 0.45 cm upstream. As a fluid element approaches the contraction, it then begins to stretch more rapidly before passing through a maximum extension rate of $\dot{\epsilon} = 1.36\ s^{-1}$ for the PTT predictions and $\dot{\epsilon} = 1.31\ s^{-1}$ for the GNF predictions. Further comparisons between the two models show that the increase in the extension rate is more acute for the GNF model than the PTT model. This observation is best explained by the tapered streamlines first shown in Figure 10a. The flow tapering leads to a gradual increase in the extension rate as the fluid element passes through the contraction rather than a sharp increase. Although the planar stresses show similar trends, the magnitudes of the net stress are substantially different. The PTT model-predicted planar stress for the LDPE resin is 130% greater than that of the GNF predictions at their peak extension rates near $y = -0.5$ cm. This difference is due to the strain-hardening behavior predicted by the PTT constitutive model.

The model predictions for LLDPE are illustrated in Figure 12. In this case, one clearly notices the strong similarity be-

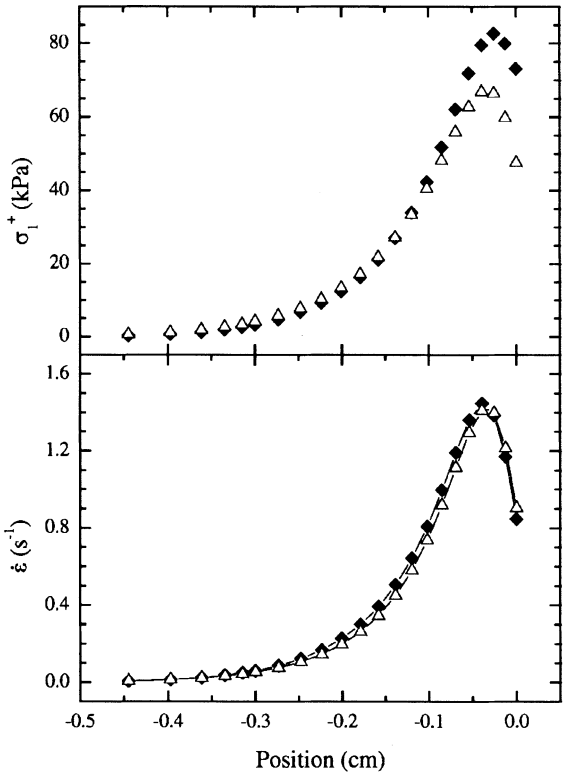

Figure 12. Predicted extension rates and extensional stresses along the plane of symmetry for LLDPE for $\dot{\gamma}_a = 8.55\ s^{-1}$.

(♦) PTT predictions, (△) GNF predictions. Lines have been drawn to aid the eye.

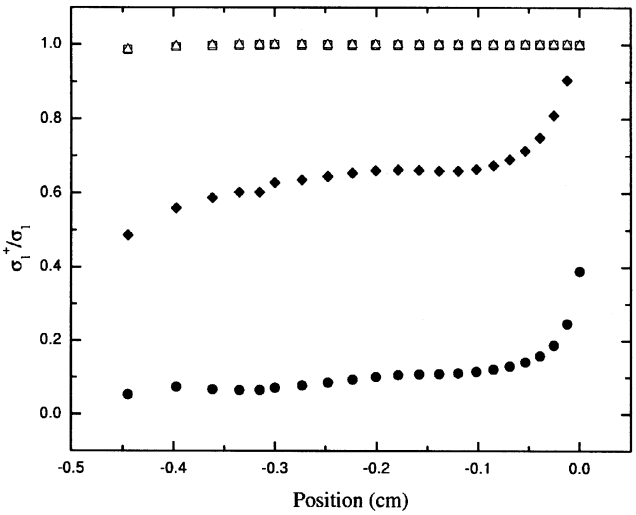

Figure 13. Normalized planar extensional stresses (σ_1^+/σ_1) along the plane of symmetry for $\dot{\gamma}_a = 8.55\ s^{-1}$.

LDPE: (●) PTT predictions, (□) GNF predictions; LLDPE: (♦) PTT predictions, (△) GNF predictions.

tween the PTT and GNF model predictions. The predicted planar extension rates are in good agreement. The increase, maximum, and a decrease in $\dot{\epsilon}$ as a function of position are almost equivalent. This is markedly different from the predictions observed for LDPE. These similarities in the extension rates concur with the streamline patterns previously seen in Figure 10b. Although there is considerably less disparity in the predicted planar stresses for LLPDE compared to those of LDPE, they do exhibit some differences at the peak extension rate near $y = -0.025$ cm. The PTT predictions are approximately 25% greater than the GNF predictions. This can be attributed to the slight differences in the extensional characteristics of the two constitutive models. This may also explain the 5% difference in the pressure profiles presented in Figure 7.

The planar stresses presented in Figures 11 and 12 represent nonsteady values of σ_1. Because fluid memory slows the growth to steady state, the influence of strain hardening is not readily apparent. Figure 13 presents the normalized values of the planar stresses (σ_1^+/σ_1) as a function of position. The steady-state predictions of σ_1 were calculated for homogenous planar extension using the predicted extension rates appearing in Figures 11 and 12. First, it is readily observed from Figure 13 that the unsteady planar stresses predicted by the PTT model for LDPE are considerably less than the steady-state planar stresses. On average, σ_1^+ is less than 10% of the steady-state value. On the other hand, the PTT model predictions for LLDPE are much closer to steady state with σ_1^+ approaching 60% of its steady-state value. The sudden upturn in normalized stresses at the contraction is a result of the decrease in the extension rate observed in Figures 11 and 12, combined with the slow relaxing behavior of the fluid. Finally, the GNF model predictions attain steady state almost instantly. This behavior is expected from an inelastic constitutive model with instantaneous fluid response. Therefore, one clearly observes from Figure 13 the influence that fluid memory can also have on the predicted stresses along the plane of symmetry.

The results obtained from analyzing the plane of symmetry suggest that the extensional characteristics of the polymer liquid are important, but may be obscured by the melt relaxation behavior in the case of a 4:1 contraction. In light of the fact that the predicted pressure profiles for LDPE were consistently lower than the measured quantities, one concern was that the PTT model parameters were not accurately predicting the extensional properties of LDPE. More specifically, in this study it was chosen to use a single value of ϵ common to all modes and then to fit that parameter using uniaxial extensional data obtained at 1.0 s^{-1}. Although this approach may lead to poor predictions at lower extension rates, it was determined that fitting to the highest available extension rate was most relevant to predicting the pressure profiles at the higher flow rates used here. In order to confirm this idea, model fitting of the ϵ parameter was performed using extensional data obtained at $\dot{\epsilon} = 0.01$, 0.1, and 1.0 s^{-1}. The corresponding values of ϵ were determined to be 10^{-6}, 0.021, and 0.034, respectively. From those parameters, the transient planar extensional viscosities were calculated as a function of strain at a planar extension rate of 1.0 s^{-1}. The calculated results are presented in Figure 14. One notices that the observed extensional viscosities increase with decreasing values of ϵ. Again, it should be noted that $\epsilon = 0.034$ refers to data obtained at 1.0 s^{-1}. Therefore, at high strains variations in

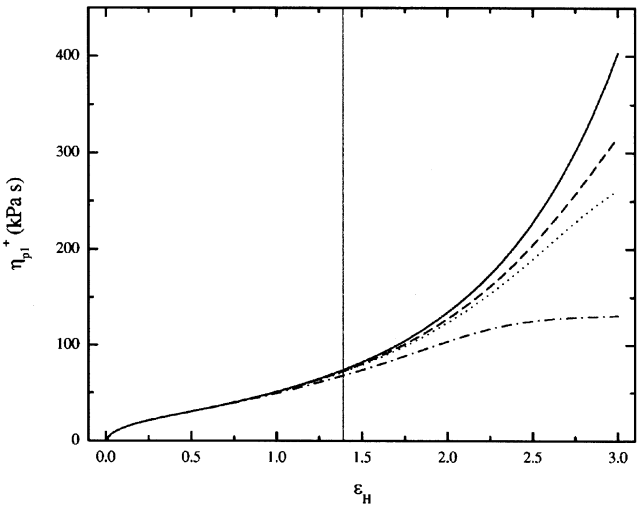

Figure 14. Calculated planar extensional viscosities (η_{p1}^{+}) as a function of strain (ϵ_H) at an extension rate of $\dot{\epsilon} = 1.0\ s^{-1}$ and different values of the PTT ϵ parameter.

$\epsilon = 1.28 \cdot 10^{-6}$ (——), 0.021 (— — —), 0.034 (···), and an arbitrary value of 0.100 (— · —).

the extensional viscosities are observed, and these variations *could* give rise to different pressure-profile predictions. However, a fluid element passing through a 4:1 contraction will experience a maximum, accumulated strain of only 1.39 strain units along the plane of symmetry. This can be calculated by the simple relation, $\epsilon_H = \ln\ \beta$, where β is the planar contraction ratio. From Figure 14, the differences in the planar extensional viscosities associated with $\epsilon_H = 1.39$ are found to be less than 9%. This relative insensitivity to ϵ was also observed for the calculated extensional viscosities at $\varphi = 0.01$ and 0.1 s^{-1} and the corresponding pressure profiles and streamline patterns predicted from simulations (not shown for brevity) (Doerpinghaus, 2002). Therefore, the influence of parameter fitting and the accuracy of the extensional viscosity predictions at high strains, or even steady state, are not as important as at small strains. Of course, this fortuitous result may not apply at larger contraction ratios in which the total strain is larger.

Conclusions

Experiments and numerical simulations have been performed for the planar contraction flow of two polyethylene melts. The influence of fluid properties, primarily extensional strain-hardening behavior, on the measured and predicted pressure profiles along a 4:1 abrupt planar contraction has been investigated. Of particular interest was whether numerical predictions could accurately predict a macroscopic quantity such as the hydrodynamic pressure along the contraction die. This ability is fundamental to die design and necessary during extrusion operations.

The accuracy of the predicted pressure profiles was found to depend on the fluid characteristics. Numerical predictions for the LDPE resin were consistently lower than the experimental values. At the highest convergent (viscoelastic) apparent shear rate of $\dot{\gamma}_a = 8.55\ s^{-1}$, both the PTT and GNF models underpredicted the pressure profiles by more than 12%. Although the PTT model predictions were somewhat greater than the GNF predictions, the effects of extensional strain hardening were not readily apparent. On the other hand, the numerical predictions for the LLDPE resin were more accurate. The PTT and GNF model predictions were within 5% of the experimental values at $\dot{\gamma}_a = 8.55\ s^{-1}$. In fact, the GNF predictions were arguably more accurate than the PTT model predictions. At higher rates, the possible effects of melt fracture and wall slip led to an overprediction of the upstream pressure values by both constitutive models. In the case of LLDPE, the onset of melt fracture corresponded well with a predicted wall shear stress, τ_w, in excess of 0.1 MPa, thus making τ_w a good numerical indicator for the presence of physical instabilities at high flow rates.

The predicted streamline patterns and the extensional properties along the plane of symmetry clearly indicate that fluid relaxation behavior and extensional strain hardening influence the flow kinematics in the entry region. Pronounced tapering of the flow into the abrupt contraction with the presence of sizable recirculating corner vortices are predicted for the LDPE material. Conversely, streamlines for the LLDPE material are very similar to the GNF predictions and the size and magnitude of the corner vortex is substantially smaller. The extensional deformation along the plane of symmetry suggests that the fluid relaxation behavior negates the effects of extensional strain-hardening behavior in the contraction region. LDPE, exhibiting a long characteristic relaxation time and high degree of extensional strain hardening, attains only 10% of the steady-state planar extensional stress as it passes through the contraction region. LLDPE, which exhibits a shorter relaxation time and extensional strain-softening behavior, attains 60% of its steady-state stress. Thus, the relaxation behavior of the polymer melt limits the magnitude of the planar extensional stress developed through a 4:1 contraction.

The relatively small extensional strains encountered along the plane of symmetry for an abrupt 4:1 planar contraction do not give rise to a significant extensional response. This is confirmed by the relative insensitivity of the predicted values to variations in nonlinear extensional parameter ϵ for the PTT model. This fortuitous response may also explain the similarities exhibited by the PTT and GNF model predictions despite variations in the predicted flow kinematics. Additional studies investigating larger contraction ratios or other flow geometries that give rise to large extensional strains should be performed to assess the significance of extensional strain hardening on pressure-profile predictions. In the case of the 4:1 planar contraction studied here, the underpredicted pressure profiles for LDPE are not completely understood, but could be elucidated further using full-field flow birefringence and velocimetry measurements of the contraction region.

Acknowledgments

The authors thank A. Willem deGroot at the Dow Chemical Company for providing the LCB and MWD data. The authors are also grateful to the Exxon Mobil Chemical Company and the Equistar Chemical Company for graciously donating their respective PE resins to this study.

Literature Cited

Ahmed, R., R. F. Liang, and M. R. Mackley, "The Experimental Observation and Numerical Prediction of Planar Entry Flow and Die Swell for Molten Polyethylenes," *J. Non-Newtonian Fluid Mech.*, **59**, 129 (1995).

Ahmed, R., and M. R. Mackley, "Experimental Centerline Planar Extension of Polyethylene Melt Flowing into a Slit Die," *J. Non-Newtonian Fluid Mech.*, **56**, 127 (1995).

Bagley, E. B., "End Corrections in the Capillary Flow of Polyethylene," *J. Appl. Phys.*, **28**, 624 (1957).

Ballenger, T. F., and J. L. White, "An Experimental Study of Flow Patterns in Polymer Fluids in the Reservoir of a Capillary Rheometer," *Chem. Eng. Sci.*, **25**, 1191 (1970).

Barakos, G., and E. Mitsoulis, "Numerical Simulation of Extrusion through Orifice Dies and Prediction of Bagley Correction for an IUPAC-LDPE Melt," *J. Rheol.*, **39**, 193 (1995).

Beraudo, C., T. Coupez, A. Fortin, Y. Demay, B. Vergnes, and J. F. Agassant, "Viscoelastic Computations in 2-D Flow Geometries," *Proc. Int. Congr. on Rheology*, Quebec City, P.Q., Canada, p. 417 (1996).

Bernstein, B., E. Kearsley, and L. Zapas, "A Study of Stress Relaxation with Finite Strain," *Trans. Soc. Rheol.*, **7**, 391 (1963).

Binding, D. M., "An Approximate Analysis for Contraction and Converging Flows," *J. Non-Newtonian Fluid Mech.*, **27**, 173 (1988).

Bird, R. B., R. C. Armstrong, and O. Hassager, *Dynamics of Polymeric Liquids*, Vol. 1: *Fluid Mechanics*, 2nd ed., Wiley, New York (1987).

Boger, D. V., "Viscoelastic Flows through Contractions," *Annu. Rev. Fluid Mech.*, **19**, 157 (1987).

Carreau, P. J., "Rheological Equations from Molecular Network Theories," PhD Diss., Univ. of Wisconsin, Madison (1968).

Chang, S.-Y., "Use of Hole Pressure Data to Obtain N_1 at High Shear Rates for Polymer Melts," Masters Thesis, Virginia Tech, Blacksburg, VA (1986).

Cogswell, F. N., "Measuring the Extensional Rheology of Polymer Melts," *Trans. Soc. Rheol.*, **16**, 383 (1972).

Den Otter, J. L., "Mechanisms for Melt Fracture," *Plast. Polym.*, **38**, 155 (1970).

Doerpinghaus, P. J., "Flow Behavior of Sparsely Branched Metallocene-Catalyzed Polyethylenes," PhD Diss., Virginia Tech, Blacksburg, VA (2002).

Dupont, S., and M. J. Crochet, "The Vortex Growth of a KBKZ Fluid in an Abrupt Contraction," *J. Non-Newtonian Fluid Mech.*, **29**, 81 (1988).

Franck, A., and J. Meissner, "The Influence of Blending Polystyrenes of Narrow Molecular Weight Distribution on Melt Creep Flow and Creep Recovery in Elongation," *Rheol. Acta*, **23**, 117 (1984).

Hatzikiriakos, S. G., and E. Mitsoulis, "Excess Pressure Losses in the Capillary Flow of Molten Polymers," *Rheol. Acta*, **36**, 545 (1996).

Kaye, A., "Non-Newtonian Flow of Incompressible Fluids," Note No. 134, College of Aeronautics, Cranfield (1962).

Laun, H. M., and H. Schuch, "Transient Elongational Viscosities and Drawability of Polymer Melts," *J. Rheol.*, **33**, 119 (1989).

Luo, X.-L., and E. Mitsoulis, "A Numerical Study of the Effect of Elongational Viscosity on Vortex Growth in Contraction Flows of Polyethylene Melts," *J. Rheol.*, **34**, 309 (1990).

Marchal, J. M., and M. J. Crochet, "A New Mixed Finite Element for Calculating Viscoelastic Flow," *J. Non-Newtonian Fluid Mech.*, **26**, 177 (1987).

Martyn, M. T., C. Nakason, and P. D. Coates, "Flow Visualization of Polymer Melts in Abrupt Contraction Extrusion Dies: Quantification of Melt Recirculation and Flow Patterns," *J. Non-Newtonian Fluid Mech.*, **91**, 109 (2000).

McLeish, T. C. B., and R. G. Larson, "Molecular Constitutive Equations for a Class of Branched Polymers: The Pom-Pom Polymer," *J. Rheol.*, **42**, 82 (1998).

Minoshima, W., and J. L. White, "A Comparative Experimental Study of the Isothermal Shear and Uniaxial Elongational Rheological Properties of Low Density, High Density and Linear Low Density Polyethylenes," *J. Non-Newtonian Fluid Mech.*, **19**, 251 (1986).

Mitsoulis, E., "Numerical Simulation of Entry Flow of the IUPAC-LDPE Melt," *J. Non-Newtonian Fluid Mech.*, **97**, 13 (2001).

Mitsoulis, E., S. G. Hatzikiriakos, K. Christodoulou, and D. Vlassopoulos, "Sensitivity Analysis of the Bagley Correction to Shear and Extensional Rheology," *Rheol. Acta*, **37**, 438 (1998).

Münstedt, H., "New Universal Extensional Rheometer for Polymer Melts. Measurements on a Polystyrene Sample," *J. Rheol.*, **23**, 421 (1979).

Münstedt, H., "Dependence of the Elongational Behavior of Polystyrene Melts on Molecular Weight and Molecular Weight Distribution," *J. Rheol.*, **24**, 847 (1980).

Münstedt, H., and H. M. Laun, "Elongational Properties and Molecular Structure of Polyethylene Melts, *Rheol. Acta*, **20**, 211 (1981).

Papanastasiou, A. C., L. E. Scriven, and C. W. Macosko, "An Integral Constitutive Equation for Mixed Flows: Viscoelastic Characterization," *J. Rheol.*, **27**, 387 (1983).

Park, H. J., D. G. Kiriakidis, E. Mitsoulis, and K.-J. Lee, "Birefringence Studies in Die Flows of an HDPE Melt," *J*. Rheol., **36**, 1563 (1992).

Petrie, C. J. S., and M. M. Denn, "Instabilities in Polymer Processing," *AIChE J.*, **22**, 209 (1976).

Phan Thien, N., "A Linear Network Viscoelastic Model," *J. Rheol.*, **22**, 259 (1978).

Phan Thien, N., and R. I. Tanner, "A New Constitutive Equation Derived from Network Theory," *J. Non-Newtonian Fluid Mech.*, **2**, 353 (1977).

Rajagopalan, D., R. C. Armstrong, and R. A. Brown, "Calculation of Steady Viscoelastic Flow using a Multimode Maxwell Model: Application of the Explicitly Elliptic Momentum Equation (EEME) Formulation," *J. Non-Newtonian Fluid Mech.*, **36**, 135 (1990).

Samurkas, T., R. G. Larson, and J. M. Dealy, "Strong Extensional and Shearing Flows of a Branched Polyethylene," *J. Rheol.*, **33**, 559 (1989).

Tanner, R. I., and K. Walters, *Rheology: An Historical Perspective*, Elsevier, Amsterdam, The Netherlands (1998).

Tuna, N. Y., and B. A. Finlayson, "Exit Pressure Experiments for Low Density Polyethylene Melts," *J. Rheol.*, **32**, 285 (1988).

White, J. L., "Experimental Studies of Elongation Flow of Polymer Melts," *Appl. Polym. Symp.*, **33**, 31 (1978).

White, J. L., and A. Kondo, "Flow Patterns in Polyethylene and Polystyrene Melts During Extrusion Through a Die Entry Region: Measurement and Interpretation," *J. Non-Newtownian Fluid Mech.*, **3**, 41 (1977).

White, S. A., and D. G. Baird, "The Importance of Extensional Flow Properties on Planar Entry Flow Patterns of Polymer Melts," *J. Non-Newtonian Fluid Mech.*, **20**, 93 (1986).

White, S. A., A. D. Gotsis, and D. G. Baird, "Review of the Entry Flow Problem: Experimental and Numerical," *J. Non-Newtonian Fluid Mech.*, **24**, 121 (1987).

Yasuda, K., R. C. Armstrong, and R. E. Cohen, "Shear Flow Properties of Concentrated Solutions of Linear and Star Branched Polystyrenes," *Rheol. Acta*, **20**, 163 (1981).

Manuscript received Sept. 2, 2002, and revision received Mar. 10, 2003.